References

[1]Marec, J. P., *Optimal Space Trajectories*, Elsevier Scientific, Amsterdam, 1979.

[2]Zondervan, K. P., and Sturgeon, S. D., "An Analytic Method for Determining Finite Burn Effects," AAS/AIAA Spaceflight Mechanics Meeting, AAS Paper 92-131, Colorado Springs, CO, Feb. 1992.

[3]Ross, I. M., "An Analysis of First-Order Singular Thrust-Arcs in Rocket Trajectory Optimization," *Acta Astronautica*, Vol. 39, No. 6, 1996, pp. 417–422.

[4]Ross, I. M., and Alfriend, K. T., "Low-Earth-Orbit Maintenance: Reboost Versus Thrust-Drag Cancellation," *Journal of Guidance, Control, and Dynamics*, Vol. 18, No. 4, 1995, pp. 930–932.

[5]McDanell, J. P., and Powers, N. F., "Necessary Conditions for Joining Optimal Singular and Nonsingular Subarcs," *SIAM Journal of Control*, Vol. 9, May 1971, pp. 161–173.

[6]Lawden, D. F., "Calculation of Singular Extremal Rocket Trajectories," *Journal of Guidance, Control, and Dynamics*, Vol. 15, No. 6, 1992, pp. 1361–1365.

Low-Thrust Orbit Raising with Coupled Plane Change and J_2 Precession

Colin R. McInnes*

University of Glasgow, Glasgow G12 8QQ, Scotland, United Kingdom

I. Introduction

MANY compact analytical expressions currently exist to describe the orbit evolution of low-thrust transfer vehicles. These expressions are particularly useful for preliminary analysis of both vehicle and mission-design concepts. In particular, compact expressions exist for both orbit radius[1,2] and polar angle,[2] along with the well-known Edelbaum solutions[3] for Δv costs during optimal transfer. These solutions have also been extended by Wiesel and Alfano.[4]

Many low-thrust transfer vehicle applications center on payload orbit raising.[5,6] For solar-electric vehicles, eclipse conditions are clearly of importance. Therefore, nodal precession is important during preliminary mission design. In addition, other applications of low-thrust transfer vehicles for polar satellite servicing[7] require the vehicle to align the nodes of its orbit with the target satellite. Again, nodal precession is clearly of significant importance for such applications.

The dynamics of a low-thrust orbital transfer vehicle are considered under the action of nodal precession caused by Earth oblateness. The vehicle also generates an out-of-plane acceleration to continuously change the orbit inclination during the transfer maneuver. Because both the transfer vehicle semimajor axis and inclination are changing, the oblateness-induced nodal precession will be strongly coupled to the orbit evolution of the low-thrust vehicle. Therefore, a set of coupled, variational equations are derived, which may be averaged to obtain the long-term evolution of the low-thrust vehicle orbit with both nodal precession and thrust-induced accelerations. The resulting coupled equations may then be solved sequentially to obtain approximate analytic solutions for semimajor axis, true anomaly, inclination, and ascending node angle, thus compactly describing the orbit evolution of the low-thrust vehicle.

II. Vehicle Dynamics

For a low-thrust-to-weight ratio vehicle with a high-specific-impulse propulsion system, the reduction in vehicle mass due to propellant depletion may be neglected. Therefore, the transfer vehicle will be modeled with a constant, thrust-induced acceleration ε.

Received June 16, 1996; revision received Jan. 16, 1997; accepted for publication Jan. 28, 1997.

*Reader, Department of Aerospace Engineering.

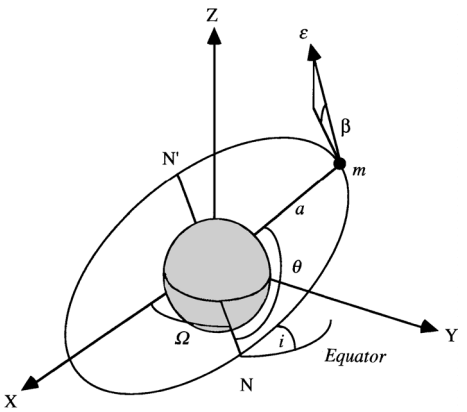

Fig. 1 Schematic orbit geometry with ascending node N and descending node N'.

This acceleration is directed along the vehicle velocity vector, but is pitched at an angle β relative to the orbit plane (Fig. 1). Again, assuming a low-thrust-to-weight ratio vehicle, the outward spiral is quasicircular. The orbit radius may then be replaced by the semimajor axis under the assumption that the orbit eccentricity is negligible. Under these conditions the Lagrange–Gauss variational equations[8] become

$$\frac{\mathrm{d}a}{\mathrm{d}t} = \frac{2\varepsilon}{\sqrt{\mu}} \cos\beta a^{\frac{3}{2}} \tag{1a}$$

$$\frac{\mathrm{d}\theta}{\mathrm{d}t} = \sqrt{\frac{\mu}{a^3}} \tag{1b}$$

$$\frac{\mathrm{d}\Omega}{\mathrm{d}t} = \varepsilon \sin\beta \sqrt{\frac{a}{\mu}} \frac{\sin\theta}{\sin i} - \frac{3}{2} \frac{\bar{n} J_2 R^2 \cos i}{a^2} \tag{1c}$$

$$\bar{n} = \sqrt{\frac{\mu}{a^3}} + \mathcal{O}(J_2)$$

$$\frac{\mathrm{d}i}{\mathrm{d}t} = \varepsilon \sin\beta \sqrt{\frac{a}{\mu}} \cos\theta \tag{1d}$$

where a represents the semimajor axis, θ the true anomaly, Ω the ascending node, i the orbit inclination, and μ the gravitational parameter. In addition, R represents the radius of the Earth and J_2 the oblateness parameter. It can be seen that Eq. (1c) contains both Earth oblateness- and thrust-induced precessions.

These equations may now be averaged with respect to true anomaly to obtain the long-period motion using the averaging operator

$$\langle z \rangle = \frac{1}{2\pi} \int_0^{2\pi} z \, \mathrm{d}\theta \tag{2}$$

Assuming that the out-of-plane thrust angle β is a function of true anomaly only and the change in elements during each orbit is small, the averaging operator may be applied to Eqs. (1) to yield

$$\left\langle \frac{\mathrm{d}a}{\mathrm{d}t} \right\rangle = \frac{\varepsilon}{\pi\sqrt{\mu}} a^{\frac{3}{2}} \int_0^{2\pi} \cos\beta(\theta) \, \mathrm{d}\theta \tag{3a}$$

$$\left\langle \frac{\mathrm{d}\theta}{\mathrm{d}t} \right\rangle = \sqrt{\frac{\mu}{a^3}} \tag{3b}$$

$$\left\langle \frac{\mathrm{d}\Omega}{\mathrm{d}t} \right\rangle = \frac{\varepsilon}{2\pi \sin i} \sqrt{\frac{a}{\mu}} \int_0^{2\pi} \sin\theta \sin\beta(\theta) \, \mathrm{d}\theta - \frac{3}{2} \frac{\sqrt{\mu} J_2 R^2 \cos i}{a^{\frac{7}{2}}} \tag{3c}$$

$$\left\langle \frac{\mathrm{d}i}{\mathrm{d}t} \right\rangle = \frac{\varepsilon}{2\pi} \sqrt{\frac{a}{\mu}} \int_0^{2\pi} \cos\theta \sin\beta(\theta) \, \mathrm{d}\theta \tag{3d}$$

These equations may now be solved by defining a suitable out-of-plane thrust angle time history. Although the equations are clearly coupled, it will be demonstrated that they may be solved sequentially to obtain compact analytical expressions.

III. Orbit Evolution

Constant Inclination

First, the thrust vector will be aligned in the orbit plane so that $\beta = 0$. The Lagrange–Gauss equations may now be solved to obtain the vehicle semimajor axis, true anomaly, and ascending node time histories. The semimajor axis may now be obtained from Eq. (3a) as a function of time by direct integration, viz.,

$$a(t) = a_0\{1 - \varepsilon\sqrt{(a_0/\mu)}t\}^{-2} \tag{4}$$

The true anomaly θ may then be obtained by substitution of Eq. (4) into Eq. (3b) with further integration yielding

$$\theta(t) = \theta_0 + \frac{1}{4(\varepsilon/g_0)}\left\{1 - \left(1 - \varepsilon\sqrt{\frac{a_0}{\mu}}t\right)^4\right\}, \qquad g_0 = \frac{\mu}{a_0^2} \tag{5}$$

where g_0 is the local gravitational acceleration at time $t = 0$. Using a similar analysis, the ascending node angle may also be obtained by substitution of the semimajor axis solution in Eq. (3c), viz.,

$$\Omega(t) = \Omega_0 + \frac{3}{16}J_2\frac{\cos i}{(\varepsilon/g_0)}\left\{\frac{R}{a_0}\right\}^2\left\{\left(1 - \varepsilon\sqrt{\frac{a_0}{\mu}}t\right)^8 - 1\right\} \tag{6}$$

A set of closed-form solutions representing the evolution of an expanding, precessing quasicircular orbit have now been obtained.

In addition to these solutions, an approximate expression for the time to escape may also be obtained. From Eq. (4) it can be seen that

$$a(t) \to \infty \qquad \text{as} \qquad t \to (1/\varepsilon)\sqrt{\mu/a_0} \tag{7}$$

However, it is clear that the escape condition will occur at a finite orbit radius so that the true escape time will be less than this limit. It can be shown that the correction factor is small for low-thrust-to-weight ratios[2] so that

$$t_{\text{esc}} \approx (1/\varepsilon)\sqrt{\mu/a_0} \tag{8}$$

In addition, the total change in true anomaly to escape can be obtained from Eq. (5) by substituting the escape time to yield

$$\Delta\theta_{\text{esc}} \approx \frac{1}{4(\varepsilon/g_0)} \tag{9}$$

as obtained in Ref. 1. Furthermore, a new expression representing the total change in ascending node angle to escape can also be obtained from Eq. (6) as

$$\Delta\Omega_{\text{esc}} \approx -\frac{3}{16}J_2\frac{1}{(\varepsilon/g_0)}\left(\frac{R}{a_0}\right)^2\cos i \tag{10}$$

It is clear from Eq. (10) that the total change in ascending node angle increases for low-thrust-to-weight ratios. This is expected as a low-thrust-to-weight ratio corresponds to a long spiral time and so a large accumulated nodal drift. More accurate solutions including a varying vehicle mass have also been derived.[9] It should be noted that for large transfer maneuvers precession due to third body effects may be significant. However, for the low-Earth orbit applications discussed in Sec. I, Earth oblateness will provide the main contribution to precession.

Variable Inclination

To model a typical transfer with out-of-plane thrust, the Edelbaum steering law[3] will be used. This corresponds to the out-of-plane thrust angle β switching between $[-\tilde{\beta}, +\tilde{\beta}]$ every half-orbit at $\theta = \pi/2$ and $3\pi/2$. Using this steering law, it is found from Eqs. (3) that

$$\left\langle\frac{\mathrm{d}\Omega}{\mathrm{d}t}\right\rangle = -\frac{3}{2}\frac{\sqrt{\mu}J_2R^2\cos i}{a^{\frac{7}{2}}} \tag{11a}$$

$$\left\langle\frac{\mathrm{d}i}{\mathrm{d}t}\right\rangle = \frac{2\varepsilon}{\pi}\sqrt{\frac{a}{\mu}}\sin\tilde{\beta} \tag{11b}$$

where the precession induced by out-of-plane thrust averages to zero. Using the semimajor axis solution, Eq. (11b) may be directly integrated by substitution to obtain

$$i(t) = i_0 - (2/\pi)\tan\tilde{\beta}\,\ell n\{1 - \varepsilon\cos\tilde{\beta}\sqrt{(a_0/\mu)}t\} \tag{12}$$

The ascending node angle may now be obtained from Eq. (11a) using the solution for semimajor axis and inclination, viz.,

$$\Omega(t) = \Omega_0 + \frac{3}{2}\frac{J_2}{(\varepsilon/g_0)\cos\tilde{\beta}}\left\{\frac{R}{a_0}\right\}^2 \times \int_{z_0}^{z}\exp\{7z\}\cos\left\{i_0 - \frac{2}{\pi}\tan\tilde{\beta}\;z\right\}\mathrm{d}z \tag{13a}$$

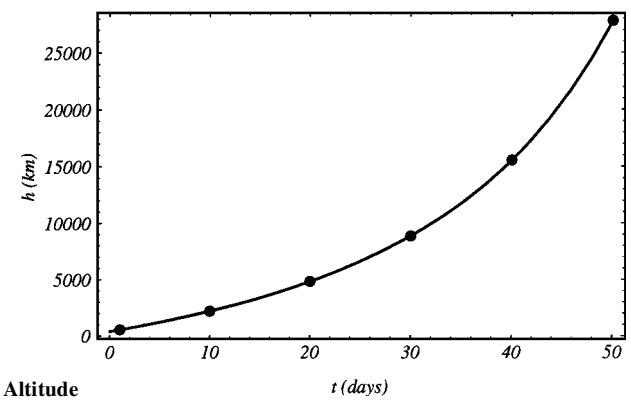

Altitude

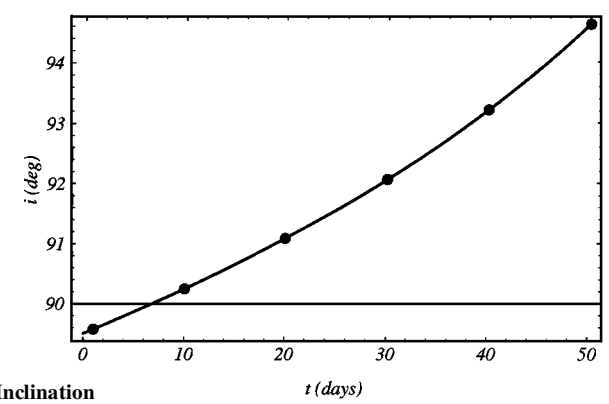

Inclination

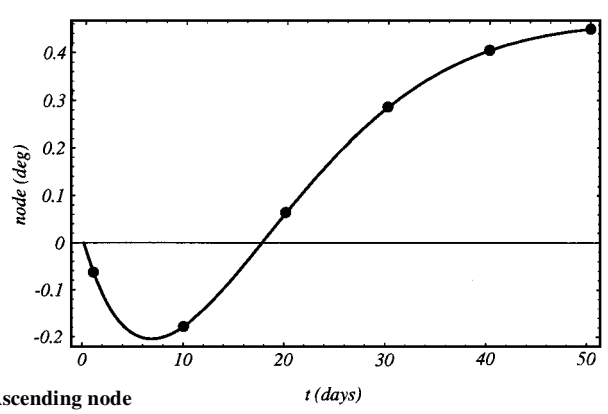

Ascending node

Fig. 2 Time history: ●, numerical integration.

where

$$z = \ell_n\{1 - \varepsilon \cos\tilde{\beta}\sqrt{(a_0/\mu)}t\} \tag{13b}$$

It is found that Eq. (13a) may then be integrated by parts to yield

$$\Omega(t) = \Omega_0 + \frac{3}{2}\frac{J_2}{(\varepsilon/g_0)\cos\tilde{\beta}}\left\{\frac{R}{a_0}\right\}^2 \{\exp\{8z\}[8\cos(mz + i_0) + m\sin(mz + i_0)] - [8\cos(i_0) + m\sin(i_0)]\} \tag{14a}$$

where

$$m = -(2/\pi)\tan\tilde{\beta} \tag{14b}$$

A set of closed-form solutions representing the evolution of an expanding, precessing quasicircular orbit with continuous plane change have now been obtained. These solutions will now be used in an illustrative example.

IV. Example: Low-Thrust Spiral

To illustrate the use of the solutions, a simple spiral maneuver will be investigated. A low-thrust vehicle with an acceleration ε of 1 mm s^{-2} will be considered with an initial altitude of 400 km and an inclination of 89.5 deg. The Edelbaum steering law will be used with $\tilde{\beta} = 10$ deg to increase the orbital inclination as the vehicle sprials outward.

The change in elements is shown in Fig. 2 over a period of 50 days. Numerical solutions obtained from the full nonlinear dynamics are also shown for comparison. It can be seen that the nodal rate changes sign as the vehicle orbit becomes retrograde. In addition, the increase in ascending node slows as the vehicle altitude increases. This is due to the strong coupling of nodal rate to semimajor axis. The total change in ascending node angle is seen to be small due to the high initial inclination. However, for lower inclinations substantial changes in ascending node angle can accumulate.[9] It can be seen that the analytic solutions prove accurate and capture coupling effects in the dynamics such as nodal rate reversals.

V. Conclusions

The dynamics of a low-thrust orbital transfer vehicle under the action of Earth-oblateness perturbations has been considered. A set of coupled, orbit-averaged equations have been derived, which may be solved sequentially. Analytic solutions for semimajor axis, true anomaly, inclination, and ascending node angle have been obtained. These solutions extend previous, well-known solutions for low-thrust spiral motion and may be used for mission analysis and design purposes.

References

[1]Wakker, K. E., *Rocket Propulsion and Spaceflight Dynamics*, Pitman, London, 1984, pp. 462–479.

[2]Wiesel, W. E., *Spaceflight Dynamics*, McGraw–Hill, New York, 1991, pp. 89–91.

[3]Edelbaum, T. E., "Propulsion Requirements for Controllable Satellites," *American Rocket Society Journal*, Vol. 31, No. 8, 1961, pp. 1079–1089.

[4]Wiesel, W. E., and Alfano, S., "Optimal Many-Revolution Orbit Transfer," *Journal of Guidance, Control, and Dynamics*, Vol. 8, No. 1, 1985, pp. 155–157.

[5]Martin, A. R., and Cresdee, M. T., "The Use of Electric Propulsion for Low Earth Orbit Spacecraft," *Journal of the British Interplanetary Society*, Vol. 41, June 1988, pp. 175–182.

[6]Deinninger, W. D., and Vondra, R. J., "Electric Propulsion for Constellation Deployment and Spacecraft Maneuvering," *Journal of Spacecraft and Rockets*, Vol. 26, No. 5, 1989, pp. 352–357.

[7]Welch, C. S., "Servicing Polar Platforms Using Low-Thrust Propulsion," 44th International Astronautical Federation Congress, IAF-93-A.6.54, Graz, Austria, Oct. 1993.

[8]Roy, A. E., *Orbital Motion*, Adam Hilger, Bristol, England, UK, 1992, pp. 183–186.

[9]McInnes, C. R., "Low-Thrust Orbit Raising with J_2 Precession," Dept. of Aerospace Engineering, Rept. 9608, Univ. of Glasgow, Scotland, UK, May 1996.

Path Planning for Space Manipulators to Reduce Attitude Disturbances

Hiroshi Okubo,* Nobuo Nagano,† Nobuo Komatsu,‡ and Toshihiro Tsumura§
Osaka Prefecture University, Sakai, Osaka 593, Japan

Introduction

FOR future activities in space, the role of robotic manipulators carried by a spacecraft will be important and it has received considerable attention. However, for practical applications, there will be many dynamic and control problems due to the dynamic coupling between the manipulator arm and the spacecraft main body. The attitude of the spacecraft will be disturbed by movement of a manipulator whereas steady-state condition is desirable for many reasons such as keeping communication links and using vision systems. A number of studies have analyzed the dynamic coupling problems and proposed methods of planning the path of space manipulators from the above point of view.[1,2] Dubowsky and his group developed an approach to the manipulator path planning that gives minimum disturbance to the spacecraft attitude.[3,4] This approach makes use of an aid called a disturbance map (DM) or enhanced disturbance map (EDM). They proposed a method for planning the minimum-disturbance manipulator path that gives the minimum fuel consumption for attitude control. This approach is most attractive for its simplicity although it assumes the use of the attitude control system for the spacecraft main body. Moreover, the applications are restricted to two- or three-link manipulators because the planning procedure requires joint space visualization and ad hoc decisions. This Note proposes a new method for planning the manipulator path using an algorithm based on the concept of EDM. The method sequentially determines the direction of joint movements in the joint space that simultaneously minimizes the disturbance to the spacecraft attitude and realizes the desired terminal joint angles.

EDM

We here consider a space robot system in two-dimensional space. When there are no external forces and torque, with zero initial angular momentum, the conservation of the angular momentum provides the relation between the spacecraft attitude variation $\delta\chi$ and the small angular movements of the manipulator joints $\delta\boldsymbol{q}$. This relation enables us to draw an EDM[4] for the method of path planning. The EDM shows the direction of joint movements, at each point in the joint space, that causes zero disturbance to the spacecraft attitude due to the manipulator motion as well as the magnitude of the maximum attitude disturbance. Figure 1 shows an example of EDM for a planner space robot with a two-link manipulator. The plotted lines are zero-disturbance lines along which attitude disturbance is zero, and the contour map shows magnitude of the maximum disturbance. The darker area of the contour map shows the higher magnitude of the maximum disturbance. The feature of the EDM varies depending on the specific mass and length parameters of the bodies in the system.

Presented as Paper 95-3338 at the AIAA Guidance, Navigation, and Control Conference, Baltimore, MD, Aug. 7–10, 1995; received Sept. 8, 1995; revision received Dec. 17, 1996; accepted for publication Dec. 26, 1996.

*Associate Professor, Department of Aerospace Engineering. Member AIAA.

†Graduate Student; currently Research Engineer, Sumitomo Precision Products Co., Ltd., Amagasaki 660, Japan.

‡Research Associate; currently Assistant Professor, Shizuoka Institute of Science and Technology, Fukuroi 437, Japan.

§Professor; currently Professor, Osaka Institute of Technology, Hirakata 573-01, Japan. Member AIAA.